Available online at www.sciencedirect.com
SCIENCE DIRECT®
Journal of Magnetic Resonance 166 (2004) 202–214
JMR Journal of Magnetic Resonance
www.elsevier.com/locate/jmr

# Measurement of dipole–dipole cross-correlated relaxation in fast rotating $CH_2D$ groups

Dominique Marion*,[1]

*Institut de Biologie Structurale Jean-Pierre Ebel, CNRS-CEA-UJF, 38027 Grenoble Cedex, France*

Received 18 July 2003; revised 7 October 2003

**Abstract**

Studies of protein dynamics are key to understanding their biological function. NMR relaxation studies of proteins to date have focused primarily on characterizing backbone dynamics. In this paper, we focus on the aliphatic side-chains (Ala, Thr, Val, Leu, and Ile) with the goal of deriving dynamical information on the motion of terminal methyl groups. Dipole–dipole cross-correlated cross-relaxation is analyzed in a fast rotating $CH_2D$ group, as found in partially deuteriated proteins. In comparison with previous studies on AMX spin systems (methylene $C^{\beta}H_2$ groups), the fast rotation of the methyl group makes a number of relaxation pathways efficient, through the coherence $C_+H^1_+H^2_- + C_+H^1_-H^2_+$. Several pulse schemes were designed to evaluate these relaxation rates: the measured values are small and well predicted by taking into account the complete relaxation network, but they remain strongly influenced by $^1H$–$^1H$ relaxation with all protons in the neighborhood of the $CH_2D$ moiety. The prospects and limitations of this method are discussed in comparison with $^2H$ relaxation measurements.


*Keywords:* Dipole–dipole cross-correlation; Protein dynamics; Fast rotating $CH_3$ groups; Degenerate $AX_2$ spin system; Transverse relaxation

## 1. Introduction

Dynamic aspects of protein structures are increasingly recognized as being crucial for a description of their biological function. In this context, NMR spectroscopy is one of the most suited experimental methods for obtaining information about protein dynamics over a wide range of time scales, ranging from fast (ps–ns) [1,2] to slow [3,4] motions. Most of the studies have focused on $^{15}N$ spin relaxation measurements; this information on a per-site basis can then be used to characterize first the anisotropy of the global motion and then the local flexibility of the protein backbone [5]. A fair correlation between secondary structure and internal flexibility is generally found, with loops more flexible than α-helices and β-sheets. Relative changes in flexibility between bound and free-states of the same protein [6] are more readily interpreted than absolute values measured on a single molecule.

As compared with backbone dynamics, the motions of protein side-chains are more pronounced and heterogeneous due to their extended degrees of freedom. Moreover, the presence of various chemical moieties on the side-chains offers a wide range of potential interactions with partners (ionic interactions, hydrophobic stacking, etc.). Therefore, an understanding of side-chain motions in proteins is of potentially greater interest but their study has been hampered by a number of practical limitations. The number of well-suited two-spin systems (analogous to the backbone $^{15}N$–$^1H$ pair) are small and $^{13}C$ auto-relaxation rates are more difficult to exploit due to the complication introduced by C–C interactions [7] in uniformly $^{13}C$ labeled proteins and by $^{13}C$–$^1H$ dipole–dipole cross-correlation effects [8,9]. An alternative to the complexities associated with dipolar relaxation is deuterium relaxation, since the deuteron is a nucleus dominated by the quadrupolar interaction. Side-chain dynamics can be monitored by $^2H$ relaxation

* Fax: +33-476-88-54-94.
*E-mail address:* dominique.marion@ibs.fr.
[1] Part of this work was carried out at the Departments of Medical Genetics, Biochemistry, and Chemistry, University of Toronto, Toronto, Ont., Canada M5S 1A8.

1090-7807/$ - see front matter © 2003 Elsevier Inc. All rights reserved.
doi:10.1016/j.jmr.2003.10.013

measurements in CHD or $CH_2D$ spin systems in $^{13}C$ labeled, fractionally deuteriated molecules [10,11]. In the case of methyl groups, the sensitivity and robustness of $^2H$ and $^{13}C$ relaxation measurements have been compared in the context of deriving order parameters and time scales of the internal motions [12].

In recent years there have been an increasing number of measurements of various cross-correlated relaxation rates, either between different dipolar interactions (DD) [11,13,14] or between DD and chemical shift anisotropy [15,16]. Cross-relaxation rates offer a number of theoretical and practical advantages over auto-relaxation rates, as they arise only from specific interactions between spins and are, in certain cases, easy to "isolate" from other contributions during measurement. A number of studies focusing on DD–DD cross-correlation in methylene groups are available in the literature, using either longitudinal ($\Gamma_{C_z,C_zH_zH_z}$) or transverse ($\Gamma_{C_+,C_+H_zH_z}$) rates. In well folded proteins, the two protons of a $C^\beta H_2$ group are generally nondegenerate and their relaxation can be described by a system of three nonequivalent nuclei (AMX system) [17]. In this paper, we direct our attention to the unexplored relaxation features associated with $CH_2D$ groups as found in protein aliphatic side-chains (Ala, Leu, Val, Ile, Thr, etc.) when observed in a partially deuteriated sample. Our goal is to adapt the strategy proposed by Yang et al. [11] to the specific case of fast rotating $CH_2D$ groups: we will show in this paper that cross-correlated cross-relaxation rates for methyls are much smaller than for sterically restricted $C^\beta H_2$ moieties. These small values lead to a situation where other relaxation pathways strongly interfere with the measurement of $\Gamma_{C_+,C_+H_zH_z}$: we here report that some pathways inside the $CH_2D$ group but also auto-relaxation with external protons may lead to systematic errors.

## 2. Methodology

Yang et al. [11] have proposed the measurement of CH–CH dipole–dipole cross-correlated relaxation rates ($\Gamma_{C_+,C_+H_zH_z}$) in a $C^\beta H_2$ group by observing the relative intensity changes in the $^{13}C$ multiplet, from a 1:2:1 pattern. The transverse cross-correlated relaxation rate is given by [9,13]:

$$\Gamma_{C_+,C_+H_z^1H_z^2} = \left(\frac{\mu_0\hbar}{4\pi}\right)^2 \frac{\gamma_C^2\cdot\gamma_H^2}{r_{HC}^6}\left\{J(0)+\frac{3}{4}J(\omega_C)\right\}, \qquad (1)$$

where $J(\omega)$ is the spectral density function defined more precisely later in this paper, $r_{HC}$ the internuclear distance between the $^1H$ and $^{13}C$ nuclei, and $\gamma_C$ and $\gamma_H$ their magnetogyric ratio. Our aim is to adapt the experimental scheme proposed for sterically hindered $C^\beta H_2$ groups to fast rotating $CH_2D$ moieties as found in aliphatic side-chains in a 100% $^{13}C$-, 50% $^2H$-labeled proteins.

### 2.1. Transverse relaxation in a $CH_2D$ group

The strategy proposed by Yang et al. [11] for $C^\beta H_2$ groups relies on the assumption that the two interacting coherences $C_+$ and $4C_+H_z^1H_z^2$ are fully isolated or at least that the intervening cross-rates are much larger than the contribution from other possible pathways.

A suitable basis for the description of the transverse relaxation of a $CH_2D$ group should thus include at least all relaxation pathways between the four following $^{13}C$ coherences:

$C_+$ (in-phase $^{13}C$ coherence),
$4C_+H_z^1H_z^2$ (doubly anti-phase coherence),
$\sqrt{2}\{C_+H_+^1H_-^2 + C_+H_-^1H_+^2\}$ (zero-quantum coherences of the $^1H$ pair),
$\sqrt{2}\{C_+H_z^1 + C_+H_z^2\}$ (anti-phase coherence)

The fourth term is added because $C_+$ interconverts into $4C_+H_z^1H_z^2$ via $\sqrt{2}\{C_+H_z^1 + C_+H_z^2\}$ when the $^1J_{CH}$-coupling evolves.

For the correct derivation of the relaxation rates between these four coherences, it is essential that the selected basis spans the total spin space. The above set of operators fulfill this requirement, for an isolated $CH_2$ group (the possible contribution of other spins will be treated as external). Note that the basis has been conveniently chosen as orthonormal, with uniform $\mathrm{Tr}\{\mathbf{B}_j^\dagger|\mathbf{B}_j\}$ and $\mathrm{Tr}\{\mathbf{B}_j^\dagger|\mathbf{B}_k\} = 0$, for $j \neq k$.

For convenience, we will introduce the following short hand notation for the coherences:

| | | |
|---|---|---|
| $C_+$ | $C_+$ | or $\boldsymbol{\alpha}$ |
| $4C_+H_z^1H_z^2$ | $C_+H_zH_z$ | or $\boldsymbol{\beta}$ |
| $\sqrt{2}\{C_+H_+^1H_-^2 + C_+H_-^1H_+^2\}$ | $C_+H_+H_-$ | or $\boldsymbol{\gamma}$ |
| $\sqrt{2}\{C_+H_z^1 + C_+H_z^2\}$ | $C_+H_z$ | or $\boldsymbol{\delta}$ |

For sake of clarity, we will use a different notation for a coherence itself ($\boldsymbol{\alpha}$) and its amplitude $\bar{\boldsymbol{\alpha}}$ or $\bar{\boldsymbol{\alpha}}(t)$ at time $t$.

The need to include $C_+H_+H_-$ can be justified in the following way: in folded proteins, the chemical shifts of the $C^\beta H_2$ *proR* and *proS* protons are generally not degenerate (AMX spin system), and thus $C_+H_+H_-$ does not remain coherent with $C_+$ or $C_+H_zH_z$ long enough for relaxation to occur efficiently (secular approximation): consequently there is not interconversion between $\boldsymbol{\gamma}$ and the other terms listed above. The situation is clearly different for $CH_2D$ which is a degenerate $AX_2$ spin system: all 3 coherences $C_+$, $C_+H_zH_z$, and $C_+H_+H_-$ have the same frequency and the relaxation pathways between them become efficient.

In the absence of any cross-correlated relaxation, a $^{13}CH_2$ triplet should exhibit a 1:2:1 pattern. $C_+H_+H_-$ corresponds to the difference between the two components of the central line (singlet and triplet manifolds): however, in a $^{13}C$ spectrum, the amplitude of $C_+H_+H_-$ cannot be *directly* measured as these two lines overlap.

Werbelow and Grant [17] have introduced the notion of observable normal modes for longitudinal magnetizations. In our case, what does really matter is not whether a coherence can be directly detected, but whether it contributes to the detected signal. It will be shown below that in our experimental scheme, $C_+H_+H_-$ ($\gamma$) contributes to the $^1H$ detected signal in contrast to $C_+H_z$ ($\delta$) which does not.

The auto- and cross-relaxation rates between these four coherences are given in Table 1. Redfield relaxation theory predicts that dipole–dipole/CSA cross-correlation leads to shifts of various energy levels, a phenomenon known as dynamic frequency shifts (DFS) [18]. In the present case there is a small shift of the two components of the central line one with respect to each other. These effects have been computed for the $CH_2D$ spin system (see Table 1) to evaluate their contribution to the spin system dynamics. In view of the small magnitude of the rates of interest, the contribution of external pathways, such as DD auto-relaxation with an external proton, may influence the spin system in an effective way. Note that the contribution of external protons are exclusively found on the diagonal of the relaxation matrix. This term shares some analogy with an auto-relaxation rate, as measured by selective inversion. Relaxation between proximal protons is highly efficient in slow tumbling macromolecules as a result of the large $J(0)$ contribution. Simulations reported below (cf. Section 3.3) will show that relaxation with the protons surrounding the $CH_2D$ group cannot be neglected.

The various terms reported in Table 1 deserve a few comments. Terms associated with DD cross-correlation link not only $C_+$ and $C_+H_zH_z$ ($\alpha \leftrightarrow \beta$) but also $C_+$ and $C_+H_+H_-$ ($\alpha \leftrightarrow \gamma$). It should be noted that the first rate involves spectral density terms at low frequency ($J(0)$ and $J(\omega_C)$) while the second is comprised of terms at high frequency ($J(\omega_H)$ and $J(\omega_C \pm \omega_H)$). Their relative importance depends upon the frequency of the motions experienced by the methyl group, that can range from fast (3-fold rotation, ps-time scale) to slow (overall tumbling of the protein, ns-time scale).

The chemical shift tensor for sp3 carbons in methyl groups can be approximated as being axially symmetric with $\Delta\sigma \sim 25$ ppm [19], a small value compared to other nuclei (peptidic $^{15}N$ or aromatic $^{13}C$). The anti-phase terms ($\delta$, i.e., $C_+H_z$) are connected with other terms only if CSA–DD cross-correlation occurs. A term corresponding to DD relaxation with an external $^1H$ ($H^x$) is present in all auto-relaxation rates ($\beta, \gamma, \delta$) except in the in-phase coherence: the occurrence of a $J(0)$ term (as in $^1H$–$^1H$ nOe) makes it rather efficient. Furthermore, these 3 rates exhibit a different linear combination of $J(0)$, $J(\omega_H)$, and $J(2\omega_H)$ and are likely to interfere in a complex manner with internal relaxation pathways to be measured.

The coefficients given in Table 1 are derived from product operator computations, but do not take into account whether the coherences involved are coherent long enough to be able to cross-relax (secular approximation). Among the many possible basis sets, two could be considered in order to numerically evaluate the relaxation rates: the Cartesian product operators described above ($\alpha, \beta, \gamma, \delta$) or a basis corresponding to the individual lines of the $^{13}CH_2$ triplet (the two outer lines as well as the singlet and triplet components of the central line) ($v_1, v_2, v_3, v_4$). This second basis can be derived from the first one by the following transformation:

$$\begin{pmatrix} v_1 \\ v_2 \\ v_3 \\ v_4 \end{pmatrix} = \begin{pmatrix} 1/2 & 1/2 & 0 & -1/\sqrt{2} \\ 1/2 & -1/2 & -1/\sqrt{2} & 0 \\ 1/2 & -1/2 & 1/\sqrt{2} & 0 \\ 1/2 & 1/2 & 0 & 1/\sqrt{2} \end{pmatrix} \begin{pmatrix} \alpha \\ \beta \\ \gamma \\ \delta \end{pmatrix}.$$

The relaxation matrix was previously computed in the line basis by Kay and Bull [9] and the shared terms are in agreement with our computation in the same basis (data not shown).

In order to correctly enforce the secular approximation, the second basis is more practical: the relaxation matrix as reported in Table 1 is first transformed to the line basis ($v_1, v_2, v_3, v_4$) and any off-diagonal element *except* those connecting $v_2$ and $v_3$ are set to zero.

### 2.2. Pulse sequence

The cross-relaxation rates ($\Gamma_{C_+,C_+H_zH_z}$) have been measured using the various pulse sequences depicted in Fig. 1. Let us focus first on the sequence shown in Fig. 1A. It contains three elements: a constant time-period $2T$ from *a* to *d*, a multiplicity filter (from *e* to *g*) and a $^{13}C$–$^1H$ refocused INEPT (from *g* to the end of the sequence). During the period $2T$, the $^{13}C$ chemical shift is monitored as function of $t_1$ and the heteronuclear coupling ($^1J_{CH}$) as function of $t_2$. In addition, the $^{13}C$ magnetization also evolves due to the one bond $^{13}C$–$^{13}C$ coupling since the protein is uniformly $^{13}C$ labeled. As this experiment is implemented for aliphatic methyl groups (single $^{13}C$ neighbor), one can choose a value of $T = 1/(2J_{CC})$ to eliminate the influence of the homonuclear coupling assuming a uniform value of $^1J_{CC}$ for all residue types. After partial processing (FT along $t_1$ and $t_3$), this experiment leads to a series of HSQC spectra ($F_1$, $F_3$) that are amplitude modulated as function of $t_2$.

If dipolar cross-correlation occurs during this period $2T$, it will alter the intensity ratio within the $^{13}C$ triplet by converting in-phase coherence ($C_+$) into doubly anti-phase coherence ($C_+H_zH_z$). Note that in contrast to many heteronuclear correlation experiments, our scheme starts on $^{13}C$ by a simple 90° pulse: this leads to the simple initial conditions ($[\bar{\alpha}(0), \bar{\beta}(0)] = [1, 0]$). Cross-correlated relaxation duting period $2T$ leads to a change

Table 1
Transverse relaxation in a non-isolated $AX_2$ spin system[a]

| Coherences | Mechanisms[b] | | Relaxation[c] | | | | | | Dynamic frequency shift | | | | |
|---|---|---|---|---|---|---|---|---|---|---|---|---|---|
| | | | $J(0)$ | $J(\omega_C)$ | $J(\omega_H - \omega_C)$ | $J(\omega_H)$ | $J(\omega_H + \omega_C)$ | $J(2\omega_H)$ | $Q(\omega_C)$ | $Q(\omega_H - \omega_C)$ | $Q(\omega_H)$ | $Q(\omega_H + \omega_C)$ | $Q(2\omega_H)$ |
| $\alpha \leftrightarrow \alpha$ | CSA(C) | CSA(C) | 16 | 12 | | | | | 12 | | | | |
| | CH | CH | 8 | 6 | 2 | 12 | 12 | | 6 | 2 | | 12 | |
| $\alpha \leftrightarrow \beta$ | CH | $H^1H^2$ | | | | | | | | | 12 | | |
| | $CH^1$ | $CH^2$ | 8 | 6 | | | | | 6 | | | | |
| $\alpha \leftrightarrow \gamma$ | CH | $H^1H^2$ | | | | | | | | | $-6\sqrt{2}$ | | |
| | $CH^1$ | $CH^2$ | | | $\sqrt{2}$ | $6\sqrt{2}$ | $6\sqrt{2}$ | | | $\sqrt{2}$ | | $6\sqrt{2}$ | |
| $\alpha \leftrightarrow \delta$ | CSA(C) | CH | $16\sqrt{2}$ | $12\sqrt{2}$ | | | | | $12\sqrt{2}$ | | | | |
| $\beta \leftrightarrow \beta$ | $HH^X$ | $HH^X$ | 4 | | | 12 | | 24 | | | | | |
| | CSA(C) | CSA(C) | 16 | 12 | | | | | 12 | | | | |
| | $H^1H^2$ | $H^1H^2$ | | | | 12 | | | | | | | |
| | CH | CH | 8 | 6 | 2 | | 12 | | 6 | 2 | | 12 | |
| $\beta \leftrightarrow \gamma$ | $H^1H^X$ | $H^2H^X$ | $-2\sqrt{2}$ | | | $-6\sqrt{2}$ | | $-12\sqrt{2}$ | | | | | |
| | $H^1H^2$ | $H^1H^2$ | | | | $-6\sqrt{2}$ | | | | | | | |
| | CH | $H^1H^2$ | | | | | | | | | $6\sqrt{2}$ | | |
| | $CH^1$ | $CH^2$ | | | $-\sqrt{2}$ | | $-6\sqrt{2}$ | | | $-\sqrt{2}$ | | $-6\sqrt{2}$ | |
| $\beta \leftrightarrow \delta$ | CSA(C) | CH | $16\sqrt{2}$ | $12\sqrt{2}$ | | | | | | | | | |
| $\gamma \leftrightarrow \gamma$ | $HH^X$ | $HH^X$ | 10 | | | 18 | | 12 | | | | | |
| | $H^1H^X$ | $H^2H^X$ | −8 | | | −12 | | | | | | | |
| | CSA(C) | CSA(C) | 16 | 12 | | | | | 12 | | | | |
| | $H^1H^2$ | $H^1H^2$ | | | | 6 | | | | | | | |
| | CH | $H^1H^2$ | | | | −12 | | | | | | | |
| | CH | CH | | 6 | 2 | 6 | 12 | | 6 | 2 | | 12 | |
| | $CH^1$ | $CH^2$ | | −6 | | | | | −6 | | | | |
| $\gamma \leftrightarrow \delta$ | | | | | | | | | | | | | |
| $\delta \leftrightarrow \delta$ | $HH^X$ | $HH^X$ | 2 | | | 6 | | 12 | | | | | |
| | CSA(C) | CSA(C) | 16 | 12 | | | | | 12 | | | | |
| | $H^1H^2$ | $H^1H^2$ | | | | 6 | | 24 | | | | | |
| | CH | $H^1H^2$ | | | | 12 | | | | | | | |
| | CH | CH | 8 | 6 | 2 | 6 | 12 | | 6 | 2 | | 12 | |
| | $CH^1$ | $CH^2$ | 8 | 6 | | | | | 6 | | | | |

[a] The rates and shifts are computed in the following orthonormal basis: $\alpha = C_+$, $\beta = 4C_+H^1_zH^2_z$, $\gamma = \sqrt{2}\{C_+H^1_+H^2_- + C_+H^1_-H^2_+\}$, $\delta = \sqrt{2}\{C_+H^1_z + C_+H^2_z\}$.

[b] $CH^1$, $CH^2$, and $H^1H^2$ correspond to the dipolar interactions inside the $CH_2D$ group. $H^X$ is a fictious external proton, that accounts for all protons in the surrounding of the $CH_2D$ group. CH indicate the sum of the $CH^1$ and $CH^2$ interactions, when both acts in a similar manner. Contributions due to the deuterium are not included (see text).

[c] The relaxation rates can be expressed as: $\Gamma = (1/8)\xi_a \cdot \xi_b \sum_\omega (k_\omega \cdot J(\omega))$ and $k_\omega$ is given in the table. The dipolar interaction constant is given by $\xi_{dd} = (\mu_0\hbar/4\pi)(\gamma_i \cdot \gamma_j/r^3_{ij})$ and the CSA constant by $\xi_{csa} = (\omega_i \cdot \Delta\sigma_i/3)$. The dynamic frequency is given by $DFS = (1/8)\xi_a \cdot \xi_b \sum_\omega (k_\omega \cdot Q(\omega))$, where the summation is performed over nonzero frequencies. The real part of the spectral density function for a freely rotating $CH_3$ groups has been expressed by Daragan and Mayo [24] as:

$$J(\omega) = (P_2(\cos\theta_{ab}) - a^{ab}_0 \cdot S^2_{CC})\frac{2}{5}\frac{\tau_e}{1 + (\omega \cdot \tau_e)^2} + (a^{ab}_0 \cdot S^2_{CC})\frac{2}{5}\frac{\tau_c}{1 + (\omega \cdot \tau_c)^2}.$$

The imaginary part ($Q(\omega)$) can be derived by replacing the term $\tau_c$ and $\tau_e$ in the numerators of $J(\omega)$ by $\omega \times (\tau^2_c)$ and $\omega \times (\tau^2_e)$, respectively. The values of $P_2(\cos\theta_{ab})$ and $a^0_{ab}$ have been reported for the various interaction (see Table 1 of [25]). For auto-correlated CH interaction $P_2(\cos\theta_{ab}) = 1$ and $a^0_{ab} = 1/9$ and for cross-correlated CH–CH interaction, $P_2(\cos\theta_{ab}) = -1/3$ and $a^0_{ab} = 1/9$. For the DD interaction with an external proton, the two parameters cannot be defined in a general way, as they depend on the molecular geometry. The values $P_2(\cos\theta_{ab}) = 1$ and $a^0_{ab} = 1$ were arbitrarily chosen for the simulations shown in Fig. 3. Other terms are found in [25].

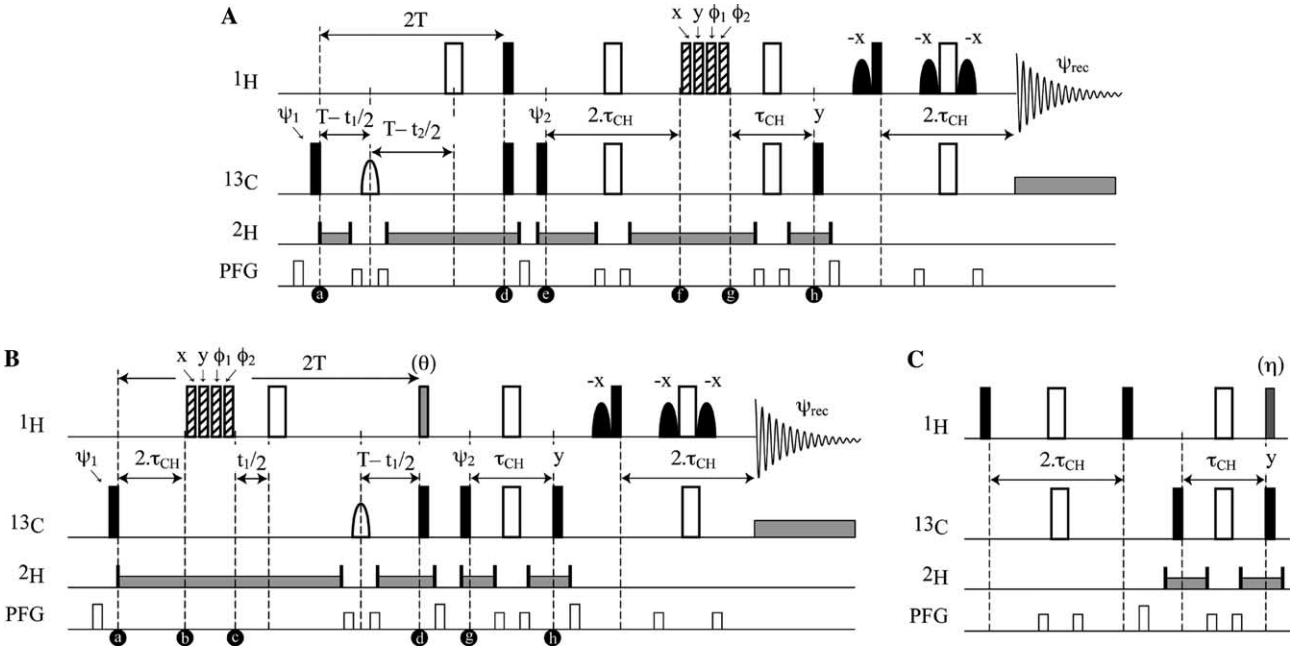


Fig. 1. Pulse sequences for the measurement of dipole–dipole (CH–CH) cross-correlated relaxation rates. Data have been recorded on a Varian INOVA spectrometer ($^1$H = 600 MHz) equipped with a triple resonance probe ($^1$H–$^{13}$C–$^{15}$N) using the standard lock channel for $^2$H decoupling. The carrier frequencies are centered at 19.4 ppm ($^{13}$C) and 4.7 ppm ($^1$H). All radio-frequency (RF) pulses are applied along the $x$ axis unless indicated. Ninety degree and 180° RF pulses are represented by filled and open symbols, respectively. All pulses (identified as rectangle) are nonselective pulses (90° ($^1$H) = 7 μs, 90° ($^{13}$C) = 13 μs), with the exception of the REBURP pulse (pulse width = 360 μs shifted to 41.1 ppm by phase modulation) on $^{13}$C (between point $a$ and $d$) and the gaussian water-selective pulse on $^1$H (pulse width = 1.2 ms) (after point $h$). The pulse field gradients are applied along the $z$-axis with a gradient strength of ≈20 G/cm and length ranging from 100 to 2000 μs. WALTZ $^2$H decoupling ($\gamma B_2 \approx 1$ kHz) is performed as long as the coherence stays on $^{13}$C (from $a$ to $h$). Both sequences lead to $^1$H–$^{13}$C HSQC type spectra where the peak intensity is modulated as function of a $^1J_{CH}$ evolution (sequence A) or the width ($\theta$°) of the gray shaded pulse (sequence B). The $^{13}$C chemical shift evolution is monitored along $t_1$ in a constant time manner during the period $2T$ (between point $a$ and $d$) where $T$ is set to a multiple value of $1/2J_{CC}$ ($J_{CC} = 35$ Hz) to refocus this homonuclear-coupling. The $^1$H chemical shift is directly detected at the end of the sequence after a reverse INEPT (starting at point $g$) optimized for $CH_2D$ groups ($\tau_{CH}$ followed by $2\tau_{CH}$ with $\tau_{CH} = 1.9$ ms $\approx 1/4J_{CH}$). The signal arising from the $CH_2D$ isotopomers is filtered by means of $2 \cdot \tau_{CH}$ ($\approx 1/2J_{CH}$) delay followed by a composite pulse 90°($x$)90°($y$)90°($\phi_1$)90°($\phi_2$). As a result of the phase cycling ($\phi_1 = y, -y$, $\phi_2 = x, -x$) this composite pulse amounts to a flip angle either 0° or 180° and the resulting signal is coadded. This filter is included with the $2T$ relaxation period in experiment B (between $a$ and $c$) and after it in experiment A (between $e$ and $g$). $^{13}$C quadrature detection is achieved in a hypercomplex manner by cycling $\psi_1$ ($= x, y$) and an additional filter (see text) is included at point $e$ ($\psi_2 = x, -x$ with $\psi_{rec} = x, -x$). Water suppression (in case of experiment recorded in $H_2O$) can be improved by adding a selective $^1$H pulse followed by a PFG at the beginning of the pulse sequence (not shown). The two pulse sequences can be modified to alter the initial conditions by adding block (C) in front of the sequence. This refocused INEPT has been optimized for $CH_2D$ groups (i.e., delay $2\tau_{CH}$ on $^1$H followed by a delay $\tau_{CH}$ on $^{13}$C). The resulting coherences at point $a$ of both sequences A and B depend on the flip angle $\eta$ of the last $^1$H (shown in gray): if $\eta = 0°$, one obtains a linear combination of $C_+$ and $C_+H_z^1H_z^2$ and if $\eta = 90°$ a combination of $C_+$ and $\{C_+H_+^1H_-^2 + C_+H_-^1H_+^2\}$ (see text for details).

of the intensity of the two coherences $\bar{\boldsymbol{\alpha}}$ and $\bar{\boldsymbol{\beta}}$ to [$\bar{\boldsymbol{\alpha}}(2T)$, $\bar{\boldsymbol{\beta}}(2T)$].

The $t_2$ modulation period—inserted inside the delay $2T$—aims at discriminating the central line of the $^{13}$C multiplet from the outter line on the basis of the $J$-coupling evolution. During $t_2$, the central line (amplitude 1/2 ($\bar{\boldsymbol{\alpha}}$ $(2T)$–$\bar{\boldsymbol{\beta}}$ $(2T)$)) does not evolve whereas the outer lines are modulated (amplitude 1/2 ($\bar{\boldsymbol{\alpha}}$ $(2T) + \bar{\boldsymbol{\beta}}$ $(2T)$)). The resulting signal is thus:

$$1/2(\bar{\boldsymbol{\alpha}}(2T) - \bar{\boldsymbol{\beta}}(2T)) + 1/2(\bar{\boldsymbol{\alpha}}(2T) + \bar{\boldsymbol{\beta}}(2T)) \times \cos(2\pi J_{CH} t_2). \quad (2)$$

Note that $C_+H_+H_-$ remains outside of this mutual exchange *due to the J-coupling* and thus does not interfere directly with this modulation. However, this does not preclude cross-relaxation with $C_+H_+H_-$ from modifying the intensity of other terms.

The two parameters extracted from experimental data by nonlinear fits (Eq. (2)) ($\bar{\boldsymbol{\alpha}}(2T)$–$\bar{\boldsymbol{\beta}}(2T)$) and ($\bar{\boldsymbol{\alpha}}(2T) + \bar{\boldsymbol{\beta}}(2T)$) are, respectively, proportional to the amplitude of the central line and of the outer lines of the $^{13}$C multiplet. The actual fitting procedure includes a possible contribution of long-range $^nJ_{CH}$-coupling (see Section 2.6): the possible line-shift between the two contributions ($v_2, v_3$) of the central line is likely to be veiled by the fitting of the $^nJ_{CH}$ contribution.

Note furthermore that only *relative* information is obtained, i.e., the amplitude of the modulated term versus that of the constant one. Thus the cross-correlated rate $\Gamma_{C_+,C_+H_zH_z}$ could be derived from the ratio of

these two terms as described by Yang et al. [11] according to:

$$\Gamma_{C_+,C_+H_zH_z} = -\frac{1}{4T}\cdot \ln\left(\frac{\bar{\alpha}(2T)+\bar{\beta}(2T)}{\bar{\alpha}(2T)-\bar{\beta}(2T)}\right). \quad (3)$$

The method proposed for $C^{\beta}H_2$ relies on the assumption that the detected signal contains only contributions from $C_+$ ($\alpha$) and $C_+H_zH_z$ ($\beta$), a very reasonable assumption for methylenes. This issue will now be discussed in the context of the relaxation of a $CH_2D$ group, where other coherences interfere (see Table 1).

Deuterium decoupling is applied throughout the delay $2T$ to prevent creation of $C_+^2H_z$ (or $C_+D_z$) antiphase magnetization and thus contribution of deuterium quadrupolar relaxation. Simulations have shown that the $^{13}C$–$^2H$ DD interaction can be neglected as a result of low magnetogyric ratio of the $^2H$ nucleus.

### 2.3. Transfer function

Let us start with the magnetization flow from the end of the $2T$ period (point *d*) up to detection: this interval can be decomposed into three interleaved elements, two projection pulses (between *d* and *e*), a multiplicity filter (between *e* and *g*) and a reversed refocused INEPT (between *g* and acquisition).

The sample is fractionally deuteriated and thus contains 4 isotopomers for the methyl groups: $CH_3$, $CH_2D$, $CHD_2$, and $CD_3$. The last species is invisible in a $^1H$ detected scheme, and the other ones can be separated on the basis of whether they are comprised of an even or odd number of protons. During a $1/2J_{CH}$ delay, the in-phase coherence $C_+$ evolves, respectively, into $C_+H_zH_zH_z$, $C_+H_zH_z$, and $C_+H_z$ for the protonated isotopomers. Applying a 180° $^1H$ pulse at the end of this delay inverts the signal only for an odd number of protons, leaving the $CH_2D$ isotopomer unmodified. In the sequences depicted in Fig. 1, this selection is performed by the group of hatched pulses (between *f* and *g* in A) which resulting flip angle is either 0° or 180° depending of the phase $\phi_1$ and $\phi_2$.

Let us turn now to the reversed focused INEPT block (between *g* and acquisition). Straightforward computation show that the $^1H$ signal detected at the end of the sequence is proportional to $\bar{\alpha}(2T)+(\bar{\gamma}(2T)/\sqrt{2})$ but not only to $\bar{\alpha}(2T)$ The $\sqrt{2}$ factor is the mere consequence of the normalization of $C_+H_+H_-$ required for computing relaxation rates.

Yang et al. [11] have emphasized the importance of the $^1H$ 90° pulse at the end of the relaxation period in their pulse sequence; along the same lines, the presence of $\gamma$ in our case is related to the $^1H$ 90° pulse at point *d*.

On this basis, the experimental information obtained from the pulse sequence in Fig. 1A is the following. We have shown that during $2T$, the $^1J_{CH}$-coupling interconverts $C_+$ and $C_+H_zH_z$ leading to a $t_2$-cosine modulated signal, which modulation amplitude is $1/2(\bar{\alpha}(2T)+\bar{\beta}(2T))$. One should remember that this amplitude is evaluated with respect to that of the non-modulated component, i.e. the amplitude for $t_2=0$. Because the $^1H$ signal detected at the very end of the pulse sequence is proportional to $\bar{\alpha}(2T)+(\bar{\gamma}(2T)/\sqrt{2})$, experiment 1A leads to the following experimental ratio:

$$R(2T)=\frac{1}{2}\frac{\bar{\alpha}(2T)+\bar{\beta}(2T)}{\bar{\alpha}(2T)+(\bar{\gamma}(2T)/\sqrt{2})}. \quad (4)$$

This equation shows that an extra term $\gamma$ interferes with the measurement of the $\Gamma_{C_+,C_+H_zH_z}$ rate. Even if $C_+H_+H_-$ is not generated at the beginning of $2T$ ($\bar{\gamma}(0)=0$), cross-relaxation may induce it during this delay, in view of the relaxation rates reported in Table 1.

While a relaxation rate can be directly derived with Eq. (3), the experimental observable $R(2T)$ (cf. Eq. (4)) cannot be converted analytically into simple relaxation rates. In contrast, from the relaxation (cross-) rates reported in Table 1, the amplitude of $\bar{\alpha}(2T)$, $\bar{\beta}(2T)$, and $\bar{\gamma}(2T)$ can be evaluated and thus $R(2T)$. In this "inverse problem," $R(2T)$ plays a pivotal role and will thus used to compare experimental and simulated data.

### 2.4. Changing initial conditions

The problem of measuring cross-relaxation during $2T$ falls into two parts: evaluating the transfer function (from *d* to the detection) and knowing the initial conditions (at point *a*). Note that in contrast to most relaxation measurements ($T_1, T_2, \ldots$), there is no way to *experimentally* determine the initial conditions $[\bar{\alpha}(0), \bar{\beta}(0), \bar{\gamma}(0), \bar{\delta}(0)]$ by setting $2T$ to 0 because the relaxation period is also used to label $^{13}C$ chemical shift and to refocus $^1J_{CC}$.

In the pulse sequence shown in Fig. 1A, the spin system is initially excited by a 90° $^{13}C$ pulse and assuming that thermal equilibrium has been previously reached, the initial conditions are $[\bar{\alpha}(0),\bar{\beta}(0),\bar{\gamma}(0),\bar{\delta}(0)] = [1.0,0,0,0]$. The pulse sequence in Fig. 1A can be modified so that different initial values are obtained. A building block based on a refocused INEPT sequence (described in Fig. 1C) can be added in front of sequence 1A. Alternatively the flip angle ($\eta$) of the $^1H$ pulse at the end of 1C can be modified to produce two different initial conditions at point *a*:

$$[\bar{\alpha}(0),\bar{\beta}(0),\bar{\gamma}(0),\bar{\delta}(0)] \sim [1.0,0.0,0.5\sqrt{2},0.0] \quad (\text{if } \eta = 90°),$$

$$[\bar{\alpha}(0),\bar{\beta}(0),\bar{\gamma}(0),\bar{\delta}(0)] \sim [1.0,1.0,0.0,0.0] \quad (\text{if } \eta = 0°).$$

The value of $0.5\sqrt{2}$ obtained in the first case results from the elimination of half of the signal by the pulse field gradient shown before point *a* (cf. Fig. 1A) (taking into account the norm of $\gamma$).

Inclusion of an INEPT building block offers advantages and drawbacks: enhanced sensitivity is obtained

due to the $^1H$–$^{13}C$ polarization transfer, but the unequal relaxation of all coherences during the INEPT element may lead to slight deviation with respect to the expected amplitudes listed above.

Alternatively, signal enhancement could be obtained by exploiting the heteronuclear nOe through $^1H$-saturation. However, this method is not compatible with our experiment: Werbelow and Grant [17] have shown that the multiplet intensity in a $AX_2$ spin system is modified by $^1H$ irradiation when cross-correlated relaxation occurs.

### 2.5. Alternate pulse sequence

In order to ascertain that the sequence shown in Fig. 1A does not lead to systematic errors, we have designed another pulse sequence to derive the same information in a different way. This sequence shown in Fig. 1B can also be combined with the INEPT building block (Fig. 1C) in an analogous manner to sequence 1A. Sequence B contains the same three elements found in sequence A, but in a different order: a constant period $2T$ from $a$ to $d$, a multiplicity filter (from $a$ to $c$) and a $^{13}C$–$^1H$ refocused INEPT (from $g$ to the end of the sequence).

During the period $2T$, the $^{13}C$ chemical shift is monitored as function of $t_1$ but—in contrast to sequence A—both hetero- ($^1J_{CH}$) and homonuclear ($^1J_{CC}$) couplings are refocused. This permits the inclusion of a multiplicity filter into the $2T$ period itself. The relaxation information is not obtained by the $^1J_{CH}$ modulation as in sequence A but from the variation of the flip angle $\theta$ at point $d$: the $^1H$ signal detected is proportional to:

$$(\bar{\boldsymbol{\alpha}}(2T) + \bar{\boldsymbol{\beta}}(2T)) + (\bar{\boldsymbol{\gamma}}(2T)/\sqrt{\mathbf{2}} - \bar{\boldsymbol{\beta}}(2T)) \sin^2\theta. \quad (5)$$

By recording to data sets with ($\theta = 0°$ and $\theta = 90°$) or monitoring the continuous variation of $\theta$ [$0° \leqslant \theta \leqslant 180°$], the following ratio can be derived for each HSQC peak after partial processing (FT along $t_1$ and $t_2$):

$$R'(2T) = \frac{\bar{\alpha}(2T) + \bar{\beta}(2T)}{\bar{\alpha}(2T) + (\bar{\gamma}(2T)/\sqrt{2})}. \quad (6)$$

Although the two experiments are based on a different type of modulation ($J$-coupling, flip angle), theory predicts that they should basically yield the same information (cf. Eqs. (4) and (6)).

### 2.6. Processing and sample

The data were acquired on a Varian INOVA spectrometer and processed using nmrPipe [20] and associated software. The 3D data sets were Fourier-transformed only along 2 of the 3 dimensions (sequence A: $(t_1, t_2, t_3) \rightarrow (F_1, t_2, F_3)$, sequence B: $(t_1, \theta, t_2) \rightarrow (F_1, \theta, F_2)$ [$0° \leqslant \theta \leqslant 180°$]). Peak intensities in these $^1H$–$^{13}C$ HSQC spectra were extracted using the non-linear spectral lineshape modeling program nLinLS [20]. These intensities were then fitted using ModelXY using appropriate mathematical models: for sequence A, a possible contribution to the $J$-modulation due to long-range $^nJ_{CH}$-couplings was included and for sequence B Eq. (5) was used.

A $^{13}C$–$^{15}N$–{50%}$^2H$ labeled sample of the 63-residue B1 immunoglobulin domain of peptostreptoccocal protein L [21] was used in this study. The sample was comprised of 1.6 mM protein, 50 mM sodium phosphate, 0.05% $NaN_3$, and 10% $^2H_2O$, pH 6.0. Measurements were carried out at 25 °C, where the overall correlation time ($\tau_c$) of protein L is 4.06 ns. Experiments were carried out with $2T = 28$ and 56 ms, but only data for the latter value are shown, which correspond to the best compromise in terms of cross-relaxation and signal-to-noise ratio.

## 3. Results and discussion

The results of the experiments carried out on protein L for $2T = 56$ ms are reported in Fig. 2. The results will be first by analyzed in an analogous fashion to a $C^\beta H_2$ group, by assuming that $\Gamma_{C_+,C_+H_zH_z}$ is larger than any other contribution. This model will be referred to as the "two coherence model," as it involves only $C_+$ and $C_+H_zH_z$.

### 3.1. The two coherence model

Data in inset 2A and 2B are first considered, derived from an experiment starting directly on $^{13}C$ (Fig. 1A). The initial value of $R$ is thus $R(0) = 0.5$. Two opposite trends are observed: for most methyl groups belonging to long side-chains (Ile and Leu) the measured ratio $R(2T)$ is larger than the starting value. At the opposite side ($R(2T) < 0.5$) are found short side-chains such as Ala and Thr. Val exhibit intermediate values between 0.48 and 0.50. A qualitative correlation emerges from these data between the measured $R$ ratio and the length of the side-chain: this tendency is expected if the length of the side-chain is prevalent in the mobility of the terminal methyl group.

Let us compare our results with the relaxation rates $\Gamma_{C_+,C_+H_zH_z}$ reported in the literature for sidechain methylene groups ($C^\beta H_2$) [11,22]. The values were obtained from the multiplet intensity using Eq. (3), where $\gamma$ does not enter. For sterically restricted methylene groups, negative $\Gamma_{C_+,C_+H_zH_z}$ value have been reported, which correspond to $R > 0.5$ (the outer lines are larger than in the absence of cross-correlation).

In the case of a sterically hindered $C^\beta H_2$, the Lipari–Szabo model-free formalism [23] was used leading to the following expression of the spectral density function:

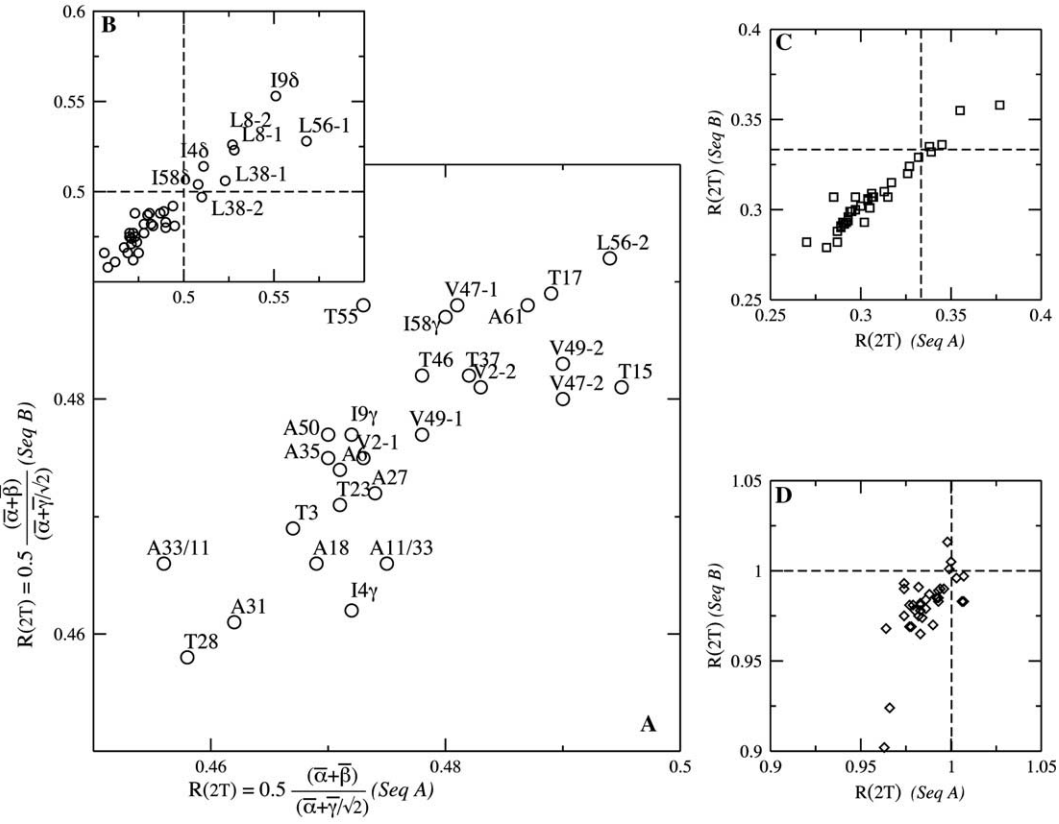


Fig. 2. Experimental data obtained for the $CH_2D$ groups of aliphatics side-chains of protein L at 25 °C. The experimental ratio

$$R(2T) = \frac{1}{2}\frac{\bar{\alpha}(2T) + \bar{\beta}(2T)}{\bar{\alpha}(2T) + (\bar{\gamma}(2T)/\sqrt{2})}$$

for a mixing time $2T = 56$ ms is shown for various experimental schemes. In each inset, the value of R obtained for the *J*-modulation scheme (sequence A) is compared with that derived from the variable-flip angle method. Inset (A) is an expansion of inset (B) for $R(2T)$ values smaller than 0.5. The data shown in the various insets correspond to different initial conditions: a simple 90° pulse is applied to the $^{13}C$ for the data in insets (A and B) $[\bar{\boldsymbol{\alpha}}(0), \bar{\boldsymbol{\beta}}(0), \bar{\boldsymbol{\gamma}}(0)] = [1.0, 0.0, 0.0]$. In the case of insets (C and D), a refocused INEPT is applied before the $^{13}C$ pulse (see caption to Fig. 1): a pair of 90° pulses on $^1H$ and $^{13}C$ is applied at the end of the refocused INEPT for inset (C) $[\bar{\boldsymbol{\alpha}}(0), \bar{\boldsymbol{\beta}}(0), \bar{\boldsymbol{\gamma}}(0)] = [1.0, 0.0, 0.5\sqrt{2}]$ while only the $^{13}C$ 90° remains for inset (D) $[\bar{\boldsymbol{\alpha}}(0), \bar{\boldsymbol{\beta}}(0), \bar{\boldsymbol{\gamma}}(0)] = [1.0, 1.0, 0.0]$. The theoretical initial value of $R$ ($R(0)$) can be computed from these coefficients and is identified by a dotted line in the plots ($R(0) = 0.5$ in insets (A and B), $R(0) = 0.333$ in (C) and $R(0) = 1.0$ in (D)). Note that in inset (B), $R(2T)$ values larger than 0.5 correspond exclusively to $CH_2D$ groups in long side-chains (Ile and Leu).

$$J(\omega) = \left[P_2\left(\cos\theta_{CH^1,CH^2}\right) - S^2_{ab}\right]\frac{2}{5}\frac{\tau_e}{1+\omega^2\tau_e^2} + S^2_{ab}\frac{2}{5}\frac{\tau_c}{1+\omega^2\tau_c^2}, \quad (7)$$

where $\tau_e^{-1} = \tau_i^{-1} + \tau_c^{-1}$, $\tau_c$ and $\tau_i$ are the correlation times of the (assumed) isotropic overall tumbling and internal motion, respectively. $S^2_{ab}$ is the order parameter as defined in the Lipari–Szabo formalism [23] extended to the case of cross-correlation between two different mechanisms ($a = CH^1$ and $b = CH^2$). In this case, $S^2_{ab}$ varies from $-1/3$ for a rigid moities to 1/9 for a unrestricted internal motion. $P_2(\cos\theta)$ is the second-order Legendre polynomial associated with $\theta_{CH^1,CH^2}$ (the angle between the two CH vectors). $P_2(\cos\theta) = -1/3$. For all $C^\beta H_2$, negative $\Gamma_{C_+,C_+H_zH_z}$ values are found which means that the first term is never large and positive enough to compensate the second negative one. Finally, one should note that the large relaxation rates measured for methylene groups can be explained very successfully with the two coherence model, as other potential terms can be safely neglected.

The model-free formalism has been extended [24,25] to the case of freely rotating $CH_3$ (or $CH_2D$) groups: 3 motions are taken into account, the 3-fold rotation of the methyl group around the C–C axis, the wobbling of this axis and the protein overall tumbling. The key assumption for the Lipari–Szabo approach is the lack of correlation between motions: the validity of such an assumption may be problematic for the the 3-fold rotation and the axis wobbling and it has been shown by $^2H$ relaxation that separating these two processes is experimentally difficult [27]. We have thus decided to use a simplier model by merging the two motions and assigning them the same correlation time $\tau_i$. Using Daragan and Mayo notation, Eq. (7) can then be rewritten by

replacing $S^2_{ab}$ by $a^0_{ab} \times S^2_{CC}$. For CH–CH cross-correlation, $a^0_{ab} = 1/9$ (see [25] for definitions and Table 1).

Assuming an overall correlation time of 4.05 ns (at 25 °C), the following values of $R(2T)$ and $\Gamma_{C_+,C_+H_zH_z}$ are obtained:

| $S^2_{CC}$ | $R(2T)$ $2T = 56$ ms | $\Gamma_{C_+,C_+H_zH_z}$ ($s^{-1}$) |
|---|---|---|
| 0.0 | 0.498 | 0.04 |
| 1.0 | 0.404 | 3.46 |

In the two coherence model, the calculated $\Gamma_{C_+,C_+H_zH_z}$ are negative for hindered $C^\beta H_2$ and positive for rotating $CH_2D$. The reversal in sign is due to the replacement of $S^2_{ab}$ by $1/9 \times S^2_{CC}$: while $S^2_{ab}$ is generally negative, $1/9 \times S^2_{CC}$ is positive. The relative contribution of the two terms in Eq. (7) is modified in favor of the second positive one. Inspection of experimental data in Fig. 2 shows that the two coherence model fails to account correctly for the relaxation in $CH_2D$ groups: the deviation from the initial value $R(0) = 0.5$ is experimentally much smaller than computed.

An internal correlation time ($\tau_i$) for both the 3-fold rotation and the C–C wobbling of 50 ps has been used: a slight increase of the computed $R(2T)$ value can be noticed if the correlation time for both motions is increased substantially (>500 ps), but such a large value is not realistic for the 3-fold rotation. $^{13}C$ $T_1$ measurement of Ala methyl groups (data not shown) leads to typical values between 1.5 and 2 s, which are incompatible with 3-fold rotations slower than 100 ps. Correlation times for 3-fold rotation of a $CH_3$ group have been evaluated from molecular dynamics simulation [26] using the AMBER force field: values ranging from 25 to 250 ps were reported but may depend on the force field used and the presence of explicit water molecules.

### 3.2. Contribution of pathways via $C_+H_+H_-$

We have shown above that additional relaxation pathways involving $C_+H_+H_-$ are required in a complete description of the relaxation in a fast rotating $CH_2D$ group. Before analyzing numerical simulations on the complete system, we will first discuss a simplified analytical derivation. The purpose of this step is to evaluate the bias due to the additional relaxation pathways. The evolution of the spin system can approximately be described by:

$$\frac{d}{dt}\begin{pmatrix}\bar{\alpha}\\ \bar{\beta}\\ \bar{\gamma}\end{pmatrix} = \begin{pmatrix} R_2 & \Gamma & \Gamma_a \\ \Gamma & R_2 & -\Gamma_a \\ \Gamma_a & -\Gamma_a & R_2 \end{pmatrix} \cdot \begin{pmatrix}\bar{\alpha}\\ \bar{\beta}\\ \bar{\gamma}\end{pmatrix}. \quad (8)$$

For simplicity, we assume that the transverse relaxation rate of the 3 coherences are the same and that $\Gamma(\alpha \leftrightarrow \gamma) \approx -\Gamma(\beta \leftrightarrow \gamma) = \Gamma_a$.

(see Table 1 for justification). If $\Gamma_a$ is small compared to ($\Gamma = \Gamma_{C_+,C_+H_zH_z}$), the eigenvalues ($\Lambda_1, \Lambda_2, \Lambda_3$) of the relaxation matrix are:

$$\Lambda_1 \approx R_2 - \Gamma - \frac{2(\Gamma_a)^2}{\Gamma}, \quad \Lambda_2 = R_2 + \Gamma,$$

$$\Lambda_3 \approx R_2 + \frac{2(\Gamma_a)^2}{\Gamma}.$$

If one computes the ratio proposed by Yang et al. [11] (cf. Eq. (3)), one obtains:

$$\frac{\bar{\alpha}+\bar{\beta}}{\bar{\alpha}-\bar{\beta}} \approx \frac{\bar{\alpha}(0)+\bar{\beta}(0)}{\bar{\alpha}(0)-\bar{\beta}(0)} \cdot \exp\left\{ -4T \cdot \Gamma \cdot \left(1 + \left(\frac{\Gamma_a}{\Gamma}\right)^2\right)\right\}. \quad (9)$$

Eq. (9) shows that the absolute value of apparent rate is always larger than the actual value $\Gamma_{C_+,C_+H_zH_z}$ when the pathways through $C_+H_+H_-$ become effective.

### 3.3. Complete numerical simulation of all pathways

The relaxation of a $CH_2D$ group can be simulated more rigorously by including all relaxation rates between the 4 coherences ($\alpha$, $\beta$, $\gamma$, $\delta$), the $J$-coupling evolution and the presence of an external proton located at a distance $r_{HX}$. We have pointed out previously that the evaluation of the relaxation rates is performed more conveniently in the basis associated with the individual lines ($v_1$, $v_2$, $v_3$, and $v_4$) in order to include the secular approximation: in this basis, all off-diagonal elements (except between $v_2$ and $v_3$) are eliminated. These simulations will serve to discuss the additional pathways inside the $CH_2D$ group and the influence of external protons. Fig. 3A shows the 3D representation of $R$ as function of the $S^2_{CC}$ order parameter and of the internuclear distance $r_{HX}$.

Let us discuss first the case where no external protons contribute ($r_{HX} > 4$ Å): the values obtained by including all coherences clearly differ from that obtained previously.

| $S^2_{CC}$ | $R(2T)$ $2T = 56$ ms | $\Gamma_{app}$ ($s^{-1}$)[a] |
|---|---|---|
| 0.0 | 0.504 | −0.13 |
| 1.0 | 0.465 | 1.24 |

[a] The notation $\Gamma_{app}$ (instead of $\Gamma$) is used to indicate that the rate is derived using equation (3) assuming that $\gamma = 0$.

Thus, the smaller range of cross-rates measured in the case of $CH_2D$ originates from the additional relaxation pathways through $C_+H_+H_-$. The numerical simulations are in agreement with the trend found earlier by the analytical computation.

It is of interest to note that the $J(\omega)$ terms present in the various rates are different: whereas the slow

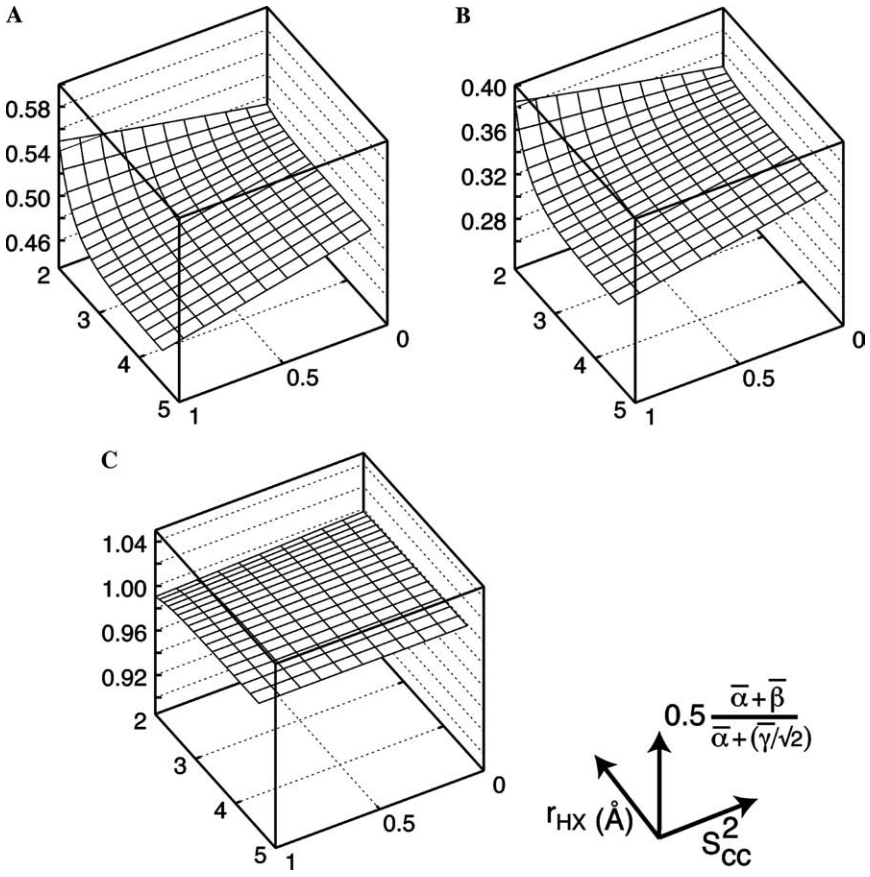


Fig. 3. Theoretical simulation of the experimental ratio

$$R(2T) = \frac{1}{2}\frac{\bar{\alpha}(2T) + \bar{\beta}(2T)}{2\bar{\alpha}(2T) + (\bar{\gamma}(2T)/\sqrt{2})}.$$

The computation were carried out using GNU Octave 2.1.40 running on Mac OS 10.2 and the plots made using GnuPlot. The relaxation rates were computed using the analytical expressions reported in Table 1, assuming a $^1$H Larmor frequency of 600 MHz and using the geometrical coefficients defined by Daragan and Mayo [25]. Starting from the initial conditions defined in the text, the spin system evolves under the influence of the $^1J_{CH}$ ($= 125$ Hz) and of relaxation ($\tau_c = 4.05$ ns, internal correlation time 50 ps, $\Delta\sigma = 25$ ppm for CSA). The $2T$ period is divided into three components (delay $2T - t_2$, 180° pulse on $^1$H and delay $t_2$) and the time evolution is obtained by diagonalizing the complete evolution matrix (relaxation and $J$-coupling). In close analogy with the experimental pulse sequence (see Fig. 1A), the intensity at the end of the $2T$ period has been evaluated for several $t_2$ values ($J$-evolution) and the ratio $R$ is derived from the intensities at $t_2 = 0$ and $t_2 = 1/4J_{CH}$. The secular approximation is enforced in the basis of the single lines (see text) by setting to zero all relaxation elements between lines at different frequencies. The imaginary components of the relaxation matrix were included in the computation, but the contribution of DFS on the final intensities turns out to be marginal. The DD interaction between the $CH_2D$ group and an external proton X was evaluated assuming a mean distance $r_{HX}$ and neglecting its modulation by the fast rotation of the methyl group. The simulation in inset (A) corresponds to an experiment beginning with a 90° pulse on $^{13}$C $[\bar{\boldsymbol{\alpha}}(0), \bar{\boldsymbol{\beta}}(0), \bar{\boldsymbol{\gamma}}(0)] = [1.0, 0.0, 0.0]$, in inset (B) and (C) with a refocused INEPT $[\bar{\boldsymbol{\alpha}}(0), \bar{\boldsymbol{\beta}}(0), \bar{\boldsymbol{\gamma}}(0)] = [1.0, 0.0, 0.5\sqrt{2}]$ and $[\bar{\boldsymbol{\alpha}}(0), \bar{\boldsymbol{\beta}}(0), \bar{\boldsymbol{\gamma}}(0)] = [1.0, 1.0, 0.0]$, respectively.

tumbling of the protein increases $J(0)$ and $J(\omega_C)$ (in $\Gamma_{C_+,C_+H_zH_z}$), the fast rotation of the methyl group enhances the higher frequency terms $J(\omega_H)$ and $J(\omega_H \pm \omega_C)$ (i.e., the other pathways $\Gamma_{C_+,C_+H_+H_-}$, etc.) In summary, the estimation of the magnitude of the various relaxation rates assuming that $J(0)$ dominates, turns out to be incorrect for fast rotating methyl groups.

The presence of an external proton in the vicinity of the methyl group has a more critical outcome: the following values are obtained for rigid side-chain ($S^2_{CC} \approx 1$):

| $r_{HX}$ | $R(2T)$ $2T = 56$ ms | $\Gamma_{app}$ ($s^{-1}$) |
|---|---|---|
| 4 Å | 0.465 | 1.24 |
| 2 Å | 0.549 | −1.76 |

In order to statically evaluate the proximity of $CH_3$ protons to external protons, we have used the crystal structure of protein L (PDB Accession Code 1HZ6) where protons have been added using standard software: more than 250 protons were found at less than 3 Å of one of the proton of the 34 methyl groups in a frozen view of the molecule (i.e., without internal motion). The

influence of external protons was thus simulated for $r_{HX}$ ranging from 2 to 5 Å (cf. Fig. 3).

The covalent geometry of 3 amino-acids raises a specific problem due to two methyls: Leu, Val, and Ile. In the first two cases, the distance between the two methyl carbons ($C^{\delta}$–$C^{\delta}$ and $C^{\gamma}$–$C^{\gamma}$) is, respectively, equal to 2.5 Å and, for Ile, can vary from 2.7 to 3.9 Å for the $C^{\delta}$–$C^{\gamma}$. In these residues as well in other (Ala and Thr), a few protons ($H^{\alpha}$, $H^{N}$) can come close to the $CH_2D$ group in a way that is highly dependent upon the local conformation and dynamics. The larger $R(2T)$ value observed for long side-chains ($R(2T) > 0.5$ see Fig. 2B) can thus be ascribed not only to higher flexibility, but also the second $CH_3$ group within the same residue contribute in the same direction. It does not seems realistic to evaluate this contribution in a $^1H$–$^1H$ NOESY experiment, as the peaks will be close to the diagonal. It should be finally noticed that the presence of $^1H$ at short distance always leads to an overestimation of the internal flexibility.

These two types of bias clearly have very different physical origins and their experimental separation might be feasible. A potential approach might be to change the initial conditions. In Figs. 2C and D are shown the experimental $R$ ratios obtained by adding an INEPT-type transfer (cf. Fig. 1C) in front of the pulse sequences (see methodology for the coefficients). The flip angle ($\eta$) actually changes the initial value from 0.33 (in Fig. 1C) to 1.00 (in Fig. 1D).

Let us first focus on Fig. 2D, where the data points clearly cluster. The corresponding simulation (Fig. 3C) shows that, in this case, $R(2T)$ is almost independent of the $S^2_{CC}$ and weakly affected by the presence of an external proton. This behavior is easily explained by the mutual cancellation of the cross-relaxation [$\alpha \rightarrow \beta$] and [$\beta \rightarrow \alpha$] when $\bar{\boldsymbol{\alpha}}(0) \approx \bar{\boldsymbol{\beta}}(0)$. The larger $R(2T)$ dispersion for Fig. 2C has been predicted (cf. Fig. 3B). In order to check whether the DD–DD cross-correlation and external $^1H$–$^1H$ DD relaxation could be separated effectively, we have searched for a linear combination of the two measurements that would be insensitive to the latter effect. As one curve can be nearly generated by homothety from the other, the combination that leads to a surface with a very small gradient along the $r_{HX}$ axis exhibits almost no variation as function of $S^2_{CC}$. This unfortunately suggests that the complete separation of DD–DD cross-correlation and external $^1H$–$^1H$ relaxation is hardly feasible in view of the experimental $S/N$ ratio of our data. This conclusion should however not be misinterpreted, as our study only shows that this

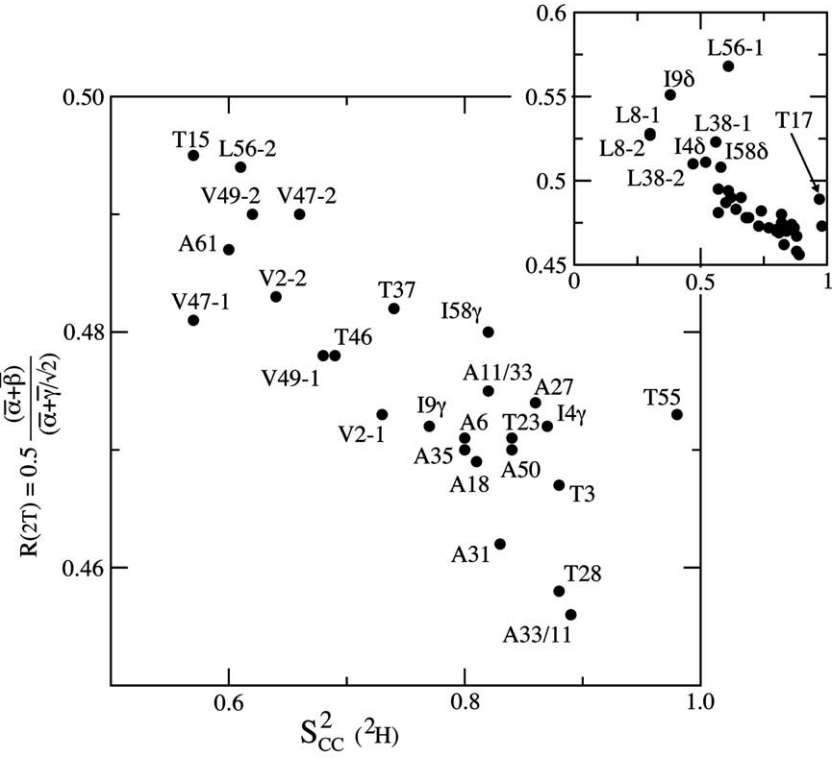


Fig. 4. Comparison of the experimental ratio $R$ obtained for Protein L (25 °C) with the $S^2_{CC}$ order parameters measured by Millet et al. [27] using a set of $^2H$ relaxation experiments. A reasonable correlation is obtained between the two parameters, although the contribution of the nOe-like effect due to extrenal protons has not been eliminated. Most of the short side-chains (such as Ala) which exhibit the same flexibility as the backbone, are found in the lower right-hand corner of the large inset ($S^2_{CC} > 0.7$ and $R(2T) < 0.48$). As discussed in the text, the effect of a close external proton leads to a larger $R(2T)$ value, or in other words an overestimation of the internal flexibility. The labels A11/33 and A33/11 refer to overlapping cross-peaks in the $^1H$–$^{13}C$ HSQC spectrum.

separation cannot be performed *with our schemes*, but does not provide in any case a definite proof that this is principally impossible.

### 3.4. Comparison with $^2H$ relaxation

We have compared the experimental data obtained from DD cross-correlated relaxation on protein L with the order parameters extracted from the $^2$H relaxation measurements [27,28]. $^2$H dynamics data for 31 out of 35 methyl groups of this proteins were well-fitted using a two-parameter Lipari–Szabo model [23], i.e., an order parameter $S^2_{CC}$ and a ps-time scale internal correlation time $\tau_i$. The 4 remaining methyl groups (T17, I4δ, and both δ-methyl groups of L8) are affected by ns time scale motion, that require a more complex fitting model [28]. Note that the $^2$H measurement leads to a $\tau_i$ mean value of 48 ps (with a standard-deviation of 22 ps), while the simulations shown in Fig. 3 have used $\tau_i = 50$ ps. The $R$ ratio obtained from DD cross-correlated relaxation (experiment starting from $^{13}$C using sequence 1A) are plotted in Fig. 4 against the $S^2_{CC}$ derived from $^2$H data [27]. The two types of information correlate reasonably well: the less flexible residues (Ala and Thr) show high $S^2$ values associated with low $R$, while most Leu and Ile cluster in the opposite corner of the plot. In the analysis of these data points it is worth pointing out that the DD cross-correlated relaxation has not been corrected from the contribution of external protons. The scattering of the data points in Fig. 4 seems to be maximal for long side-chains containing two methyls, i.e., a number of proximal $^1$H. The behavior of T17 (high $S^2_{CC}$ and $R(2T)$ value) might be due to the occurrence of ns-time scale motion (mentionned in [28]), that is likely to affect both relaxation probes differently. Inspection of the crystal structure of protein L (PDB 1HZ6) does not provide any apparent explanation for this restricted mobility, such as side-chain H-bond.

## 4. Conclusion

A new set of experiments has been proposed to utilize DD–DD cross-correlated cross-relaxation as a measure of internal mobility in aliphatic terminal $CH_2D$ groups. The cross-correlation between two CH vectors has been successfully used in the past for sterically hindered $C^\beta H_2$ groups [11]. Despite the close analogy between the two systems, major theoretical and experimental differences emerge: as a result of the fast rotation of the methyl, the apparent experimental rates for $\Gamma_{C_+,C_+H_zH_z}$ are much smaller in magnitude. A detailed analysis shows that this measurement is biased by two different effects: the cross-relaxation with $C_+H_+H_-$ and $^1$H–$^1$H auto-relaxation with all spatially close protons.

In the context of side-chain dynamics, the impact of these two problems is clearly very different: a model including all pathways inside the $CH_2D$ group remains tractable. In contrast, cross-relaxation with external protons would require the knowledge of the complete $^1$H relaxation network as well as its dynamics. This latter point shares some analogy with spin-diffusion in $^1$H–$^1$H nOe measurements, where the isolated spin pair approximation fails. If used in a qualitative manner, our experimental schemes provide however an estimate of the flexibility of the chain, though with a much smaller accuracy than previously proposed $^2$H experiments.

The complete relaxation matrix for a degenerate spin system ($AX_2$) has been derived, showing a number of key differences with a simple AMX spin system. In contrast to the real terms (line-width) that contain numerous contributions from external protons, it is noteworthy that the imaginary terms (line-shift) do not suffer from any of these external interferences. Because frequencies can be generally measured with higher accuracy than exponential decays, it might be worth exploring the potentialities of dynamic frequency shifts for backbone and side-chain dynamics, if this lack of coupling with the external "world" turns out to be a general feature.

## Acknowledgments

This work was initiated during a sabbatical stay in the laboratory of Prof. Lewis E. Kay (University of Toronto) and was supported by a grant of the France–Canada Research Fund (FCRF). The author would like to thank Prof. L.E. Kay for this continuous support and the numerous and fruitful discussions during all steps of this study. Stimulating conversations on relaxation theory with Nikolai R. Skrynnikov are also acknowledged.

## References

[1] L.E. Kay, D.A. Torchia, A. Bax, Backbone dynamics of proteins as studied by $^{15}$N inverse detected heteronuclear NMR spectroscopy: application to staphylococcal nuclease, Biochemistry 28 (1989) 8972–8979.
[2] J.W. Peng, G. Wagner, Investigation of protein motions via relaxation measurements, Methods Enzymol. 239 (1994) 563–596.
[3] M. Akke, A.G. Palmer III, Monitoring macromolecular motions on microsecond to millisecond time scales by $R_1\rho - R_1$ constant relaxation time NMR spectroscopy, J. Am. Chem. Soc 118 (1996) 911–912.
[4] A.G. Palmer III, C.D. Kroenke, J.P. Loria, Nuclear magnetic resonance methods for quantifying microsecond-to-millisecond motions in biological macromolecules, Methods Enzymol. 339 (2001) 204–238.
[5] F. Cordier, M. Caffrey, B. Brutscher, M.A. Cusanovich, D. Marion, M. Blackledge, Solution structure, rotational diffusion

anisotropy and local backbone dynamics of *Rhodobacter capsulatus* cytochrome $c_2$, J. Mol. Biol. 281 (1998) 341–361.

[6] S. Bhattacharya, M.V. Botuyan, F. Hsu, X. Shan, A.I. Arunkumar, C.H. Arrowsmith, A.M. Edwards, W.J. Chazin, Characterization of binding-induced changes in dynamics suggests a model for sequence-nonspecific binding of ssDNA by replication protein A, Protein Sci. 11 (2002) 2316–2325.

[7] T. Yamazaki, R. Muhandiram, L.E. Kay, NMR experiments for the measurement of carbon relaxation properties in highly enriched, uniformly $^{13}C$, $^{15}N$-labeled proteins: application to $^{13}C^{\alpha}$ carbons, J. Am. Chem. Soc. 116 (1994) 8266–8278.

[8] A.D Bain, R.M. Lynden-Bell, The relaxation matrices for $AX_2$ and $AX_3$ nuclear spin systems, Mol. Phys. 30 (1975) 325–356.

[9] L.E. Kay, T.E. Bull, Heteronuclear transverse relaxation in AMX, $AX_2$, and $AX_3$ spin systems, J. Magn. Reson. 99 (1992) 615–622.

[10] D.R. Muhandiram, T. Yamazaki, B.D. Sykes, L.E. Kay, Measurement of $^2H$ $T_1$ and $T_{1\rho}$ relaxation times in uniformly $^{13}C$-labeled and fractionally $^2H$-labeled proteins in solution, J. Am. Chem. Soc. 117 (1995) 11536–11544.

[11] D. Yang, A. Mittermaier, Y.K. Mok, L.E. Kay, A study of protein side-chain dynamics from new $^2H$ auto-correlation and $^{13}C$ cross-correlation NMR experiments: application to the N-terminal SH3 domain from drk, J. Mol. Biol. 276 (1998) 939–954.

[12] R. Ishima, A.P. Petkova, J.M. Louis, D.A. Torchia, Comparison of methyl rotation axis order parameters derived from model-free analyses of $^2H$ and $^{13}C$ longitudinal and transverse relaxation rates measured in the same protein sample, J. Am. Chem. Soc. 123 (2001) 6164–6171.

[13] M. Ernst, R.R. Ernst, Heteronuclear dipolar cross-correlated cross relaxation for the investigation of side-chain motions, J. Magn. Reson. 110 (1994) 202–213.

[14] B. Reif, A. Diener, M. Hennig, M. Maurer, C. Griesinger, Cross-correlated relaxation for the measurement of angles between tensorial interactions, J. Magn. Reson. 143 (2000) 45–68.

[15] M. Goldman, Interference effects in the relaxation of a pair of unlike spin-1/2 nuclei, J. Magn. Reson. 60 (1984) 437–452.

[16] B. Brutscher, N.R. Skrynnikov, T. Bremi, R. Brüschweiler, R.R. Ernst, Quantitative investigation of Dipole–CSA cross-correlated relaxation by ZQ/DQ spectroscopy, J. Magn. Reson. 130 (1998) 346–351.

[17] L.G. Werbelow, D.M. Grant, Intramolecular dipolar relaxation in multispin systems, Adv. Magn. Reson. 9 (1977) 189–299.

[18] L.G. Werbelow, NMR dynamic frequency shifts and the quadrupolar interaction, J. Chem. Phys. 70 (1979) 2329–2332.

[19] C. Ye, R. Fu, J. Hu, L. Hou, S. Ding, Carbon-13 chemical shift anisotropy of solid amino-acids, Magn. Reson. Chem 31 (1993) 699–704.

[20] F. Delaglio, S. Grzesiek, G.W. Vuister, G. Zhu, J. Pfeifer, A. Bax, NMRPipe: a multidimensional spectral processing system based on UNIX pipes, J. Biomol. NMR 6 (1995) 277–293.

[21] M.L. Scalley, Q. Yi, H. Gu, A. McCormack, J.R. Yates, D. Baker, Kinetics of folding of the IgG binding domain of peptostreptococcal protein L, Biochemistry 36 (1997) 3373–3382.

[22] L. Banci, I. Bertini, I.C. Felli, P. Hajieva, M.S. Viezzoli, Side chain mobility as monitored by CH–CH cross correlation: the example of cytochrome $b_5$, J. Biomol. NMR 20 (2001) 1–10.

[23] G. Lipari, A. Szabo, Model-free approach to the interpretation of muclear magnetic relaxation in macromolecules 1. Theory and range of validity, J. Am. Chem. Soc. 104 (1982) 4546–4559.

[24] L.E. Kay, D.A. Torchia, The effect of dipolar cross-correlation, J. Magn. Reson. 95 (1991) 536–547.

[25] V.A. Daragan, K.H. Mayo, A novel model-free analysis of $^{13}C$ NMR relaxation of alanine-methyl side-chain motions in peptides, J. Magn. Reson. 110 (1996) 164–175.

[26] S.P. Edmondson, Molecular dynamics simulation of the effects of methyl rotation and other protein motions on the NOE, J. Magn. Reson. B 103 (1994) 222–233.

[27] O. Millet, D.R. Muhandiram, N.R. Skrynnikov, L.E. Kay, Deuterium spin probes of side-chain dynamics in proteins 1. Measurement of five relaxation rates per deuteron in $^{13}C$-labeled and fractionally $^2H$-enriched proteins in solution, J. Am. Chem. Soc. 124 (2002) 6439–6448.

[28] N.R. Skrynnikov, O. Millet, L.E. Kay, Deuterium spin probes of side-chain dynamics in proteins. 2. Spectral density mapping and identification of nanosecond time-scale side-chain motions, J. Am. Chem. Soc. 124 (2002) 6449–6460.